Modeling of radial asymmetry in lens distortion facilitated by modern optimization techniques

Jason P. de Villiers[*a], F. Wilhelm Leuschner[b], Ronelle Geldenhuys[b]

[a]Council for Scientific and Industrial Research, Meiring Naude Rd, Pretoria, South Africa;

[b]Department of Electrical, Electronic and Computer Engineering, University of Pretoria, Pretoria, South Africa;

ABSTRACT

Most current lens distortion models use only a few terms of Brown's model, which assumes that the radial distortion is dependant only on the distance from the distortion centre, and an additive tangential distortion can be used to correct lens de-centering. This paper shows that the characterization of lens distortion can be improved by over 79% compared to prevailing methods. This is achieved by using modern numerical optimization techniques such as the Leapfrog algorithm, and sensitivity-normalized parameter scaling to reliably and repeatably determine more terms for Brown's model. An additional novel feature introduced in this paper is to allow the distortion to vary not only with polar distance but with the angle too. Two models for radially asymmetrical distortion (i.e. distortion that is dependant on both polar angle and distance) are discussed, implemented and contrasted to results obtained when no asymmetry is modelled. A sample of 32 cameras exhibiting extreme barrel distortion (due to their 6.0mm focal lengths) is used to show that these new techniques can straighten lines to within 7 hundredths of a pixel RMS over the entire image.

Keywords: Asymmetry, numerical optimization, distortion characterization, real-time

1. INTRODUCTION

Most optical lenses induce some amount of distortion in the images they create, that is: the resultant images differ from what one would obtain with an ideal pinhole camera. In addition to the obvious aesthetic degradation, this has severe consequences for any measurements calculated from the image and for such applications as machine vision, stitching,[1] product defect detection, remote sensing and motion tracking. While it is possible to correct all or some of the distortion optically, this increases the size, mass and price of the lenses considerably and, therefore, the correction is frequently done in software.

For spherical element lenses, it has been common practice in the literature[2,3] to model only the first few radial distortion parameters of the Conrady/Brown model.[4–6] The authors have previously shown[7] that more parameters can be reliably fitted and that doing so results in a superior characterization.

This paper shows that the Conrady/Brown model can be further extended to yield even better results. Typically the radial distortion of a lens dominates the tangential/de-centering distortion components, yet the model implies that any points on a circle centered about the distortion centre require the same radial adjustment. In other words, the angular component of the polar coordinate is irrelevant. It is shown in the rest of the paper that making the radial correction aspect of the Conrady/Brown model dependant on the polar angle can significantly improve the characterization.

The rest of this paper is organised as follows: Section 2 describes the angular warpings used, and Sec. 3 details the hardware and software setups used to test the new angle-dependent characterisation models. Section 4 both provides and discusses the results and finally Sec. 5 places this work in context and summarizes the findings.

[*]jdvilliers@csir.co.za; phone: +27 12 841 4860; www.csir.co.za

2. ANGULAR GAIN

In order to test the efficacy of incorporating an angular component for lens distortion, the Brown/Conrady model was augmented to include a polar angle dependant gain for the radial components as shown in Eq. 1.

$$\begin{aligned} x_u &= x_d + f(\theta)(x_d - x_c)(K_1 r^2 + K_2 r^4 + \ldots) + \\ &\quad \left(P_1(r^2 + 2(x_d - x_c)^2) + 2P_2(x_d - x_c)(y_d - y_c)\right)(1 + P_3 r^2 + \ldots) \\ y_u &= y_d + f(\theta)(y_d - y_c)(K_1 r^2 + K_2 r^4 + \ldots) + \\ &\quad \left(2P_1(x_d - x_c)(y_d - y_c) + P_2(r^2 + 2(y_d - y_c)^2)\right)(1 + P_3 r^2 + \ldots)) \end{aligned} \tag{1}$$

where:

(x_u, y_u) = undistorted image point,

(x_d, y_d) = distorted image point,

(x_c, y_c) = centre of distortion,

K_n = N$^{\text{th}}$ radial distortion coefficient,

P_n = N$^{\text{th}}$ tangential distortion coefficient,

$\theta = tan^{-1}\left(\frac{y_d - y_c}{x_d - x_c}\right)$

$f(\theta)$ = the radial gain,

$r = \sqrt{(x_d - x_c)^2 + (y_d - y_c)^2}$, and

$\ldots$ = an infinite series.

There are some requirements for the polar gain $f(\theta)$)in Eq. 1. Firstly, it has to be continuous over the range $[0, 2\pi]$, and that $f(2\pi) = f(0)$ so there is not a discontinuity at the wrap around. Multiple functions of this nature were derived and evaluated but only the ones that were found to be advantageous are discussed here. For instance, gains of the form given by Eq. 2 were not found to be beneficial and are not discussed further.

$$f(\theta) = c + ((\theta - \alpha) - 0) \times ((\theta - \alpha) - 2\pi) \times \Pi_{n=0}^{n<m}((\theta - \alpha) - Z_n) \tag{2}$$

where:

$f(\theta)$ = the radial gain,

α = the angular offset,

m = the number of zeroes,

n = the vertical offset, and

Z_n = the Nth zero.

2.1 Elliptical angular gain

The implicit acceptance of radial symmetry in the Conrady/Brown model implies that the lens elements are perfectly formed and have a uniform refractive index and the that imager is both perfectly orthogonal to the optical axis and perfectly planar. Whilst these criteria can indeed never strictly be met. The assumption of radial symmetry is particularly untrue for cheaper, mass-produced lenses. In particular, non-orthogonal image planes would lead to elliptical distortion as seen in Fig. 1.

The formula for the radius of an ellipse with horizontal major axis and focii equidistant from the origin is

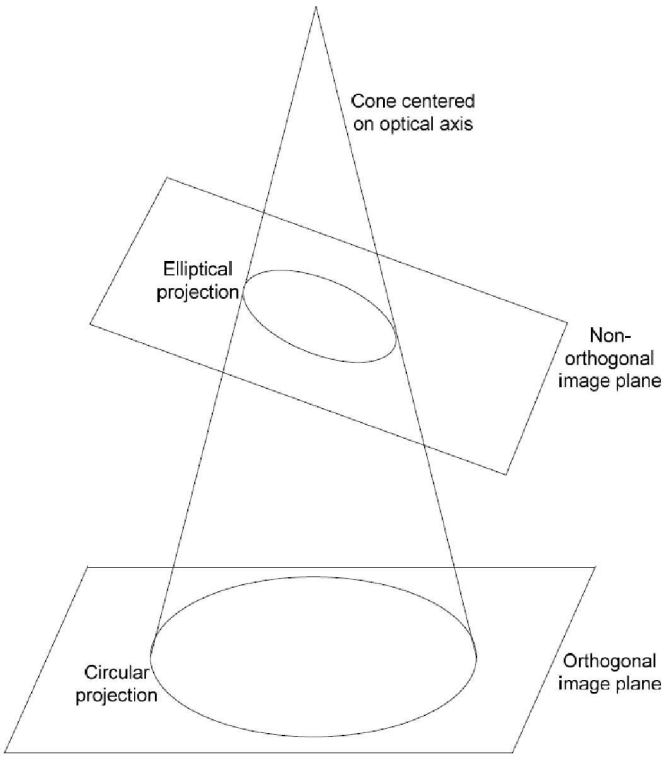

Figure 1. Elliptical projecting resulting from a non-orthogonal conic slice

given by Eq. 3.

$$r(\theta) = \sqrt{a^2 cos^2(\theta) + b^2 sin^2(\theta)} \tag{3}$$

where:

r = radius of the ellipse,

a = major (horizontal) axis of ellipse,

b = minor (vertical) axis of ellipse, and

θ = polar angle

Generalizing the major axis to be at any angle relative to the horizontal axis, and normalizing the major axis to be of unit length, as well as providing an overall gain yields the elliptical gain algorithm used in this work and given by Eq. 4.

$$f(\theta) = a\sqrt{cos^2(\theta - \alpha) + b^2 sin^2(\theta - \alpha)} \tag{4}$$

where:

θ = the polar angle,

a = the gain of the ellipse,

b = normalized minor axis of ellipse ($\in (0, 1]$), and

α = clockwise angle of major axis from horizontal.

2.2 Sinusoidal angular gain

Perhaps surprisingly, the simple fixed frequency sinusoid not only meets the criteria but performed well, in addition to being smooth on the interval. Equation 5 provides the generalized form used in this work.

$$f(\theta) = asin(\theta - \alpha) + b \tag{5}$$

where:

θ = the polar angle,

a = the gain,

b = the vertical offset, and

α = the angular offset.

3. EXPERIMENTAL SETUP

In order to verify the improved performance of the polar augmented distortion models, real world data was collected, and a metric to determine the level of distortion formulated. As this is the logical extension to the authors' previous work,[7] both the physical setup and the data set up are the same as those that were previously published. They are restated here for the purposes of completeness.

3.1 Cameras

A population of 32 cameras each with a nominal focal length of 6mm and 76° by 56° field of view (FOV) frustum (which corresponds to the outlines in Fig. 2) were used. The cameras had square pixels and orthogonal horizontal and vertical axes. The distortion induced by the cameras required a correction of more than 73 pixels, or 8.7% of the diagonal FOV in the upper right corner of Fi. 2(b). Two lens designs were considered, with 8 samples of Design A and 24 samples of Design B evaluated.

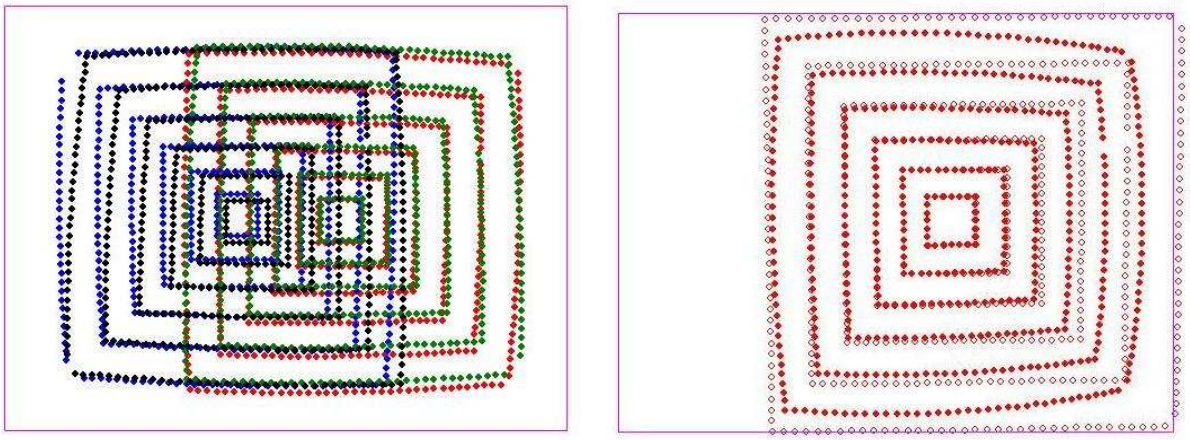

(a) Four distorted views of the reference jig

(b) Distorted and undistorted view of the reference jig

Figure 2. Optical reference jig

3.2 Optical reference jig

The cameras each captured the centroids of an optical reference jig which has 504 circular marks arranged in 6 concentric squares. Each camera captured 4 different views of the jig such that the entire field of view was covered, as illustrated in Fig. 2(a).

3.3 Distortion measure

Brown proposed the plumb-line method in 1971[6] and it has been used almost universally since. Essentially, given points along a supposed-to-be-straight line, Brown fitted the least- squares straight line through the points, the error (for that line) being the sum of the perpendicular distances from the line. A slight adaptation to the above was used in this work, whereby the perpendicular distance between the point and the line is still used, but the line is expressed in the more tractable form of a unit direction vector and a point on the line. The following equation shows the distortion metric used, which is the Root Mean Square (RMS) perpendicular distance of all the points from their corresponding lines. Note that as the jig consisted of concentric squares constructed with equidistant references, the number of references per line is not constant. In this work N was 96 (four views of six squares having the usual four sides each) and $\sum_{n=0}^{n<N} M_n > 2016$ as the corner references are used for two lines each.

$$distortion = \sqrt{\frac{1}{\sum_{n=0}^{n<N} M_n} \sum_{n=0}^{n<N} \sum_{m=0}^{m<M_n} \left((\|\bar{p_p^n} - \bar{p_l^n}\|_2)^2 - ((\bar{p_p^n} - \bar{p_l^n}) \cdot \bar{d_n})^2 \right)} \tag{6}$$

where

N = the number of straight lines in the data captured,
M_n = the number of points along the nth line,
$\bar{d_n}$ = unit direction vector of the line,
$\bar{p_l^n}$ = the point on the line, and
$\bar{p_p^n}$ = the point in question.

3.4 Skewness measure

It was seen in preliminary measurements that variable angular gains could induce a trapezoidal effect on what should have been rectangular corrected images. The metric used to quantify this effect is given by Eq. 7. It compares the variable angular gain corrections with the constant angular gain (i.e.$f(\theta) = 1$), while this will indeed highlight differences between the two it does not necessarily mean that a small skewness of one or two degrees is bad although a larger value would be a cause for concern. Figure 3 depicts a typical example of trapezoidal skewness.

$$skewness = max_i \Big[cos^{-1} \left(\frac{\bar{p}_{i,end} - \bar{p}_{i,start}}{\|\bar{p}_{i,end} - \bar{p}_{i,start}\|} \cdot \frac{\bar{q}_{i,end} - \bar{q}_{i,start}}{\|\bar{q}_{i,end} - \bar{q}_{i,start}\|} \right) \Big] \tag{7}$$

where

i = the number $\in [1, 96]$ of the line being considered,
$\bar{p}_{i,end}$ = the last existing undistorted point in the variable radial gain line,
$\bar{p}_{i,start}$ = the last first distorted point in the variable radial gain line,
$\bar{q}_{i,end}$ = the last existing undistorted point in the constant radial gain line, and
$\bar{q}_{i,start}$ = the first existing undistorted point in the constant radial gain line.

3.5 Numerical Techniques Overview

Equation 6 provides a means to quantify how much distortion a lens induces. Lower values are better, and this section describes the methods used to minimize the metric.

The Leapfrog Algorithm[8] is used in this work, since it was previously shown to provide superior characterizations and is known to be robust to noise and intractable problems[9] . It uses only gradient information to find the minimum and is thus a first order optimization technique. The algorithm simulates a particle which appears at rest at the provided starting point and is subjected to accelerations induced by the gradient of the function being minimized. It is worth noting that the acceleration induces a velocity (and therefore momentum) which

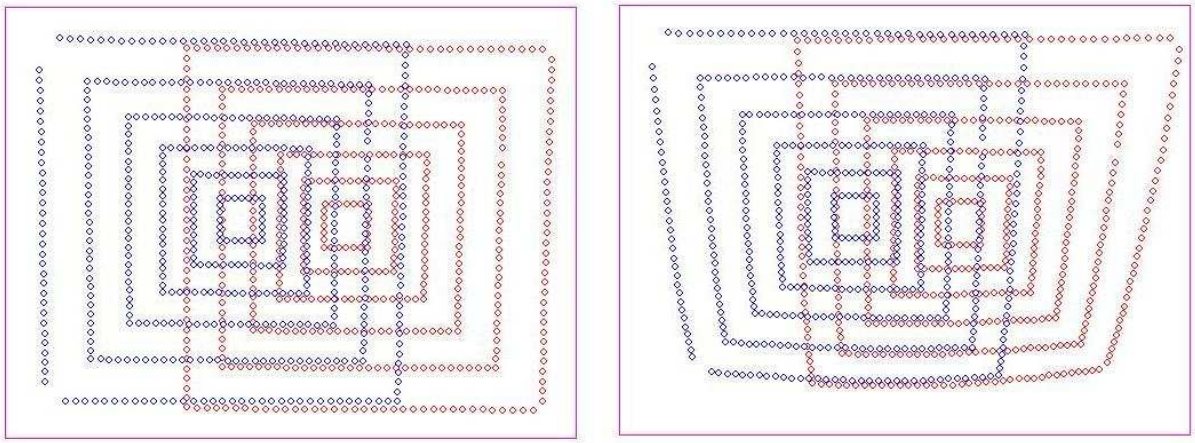

(a) No skewness evident (b) Skewness evident

Figure 3. Illustration of trapezoidal skewness

allows the particle to go over 'humps' and thus finds not the nearest local minimum, but the nearest 'low local' minimum.[8]

It is also important to scale the variables so that the gradient is equally sensitive to a step in any direction.[9] For instance the K_3 coefficient of Brown's model[5] has to have a lower scale than the K_2 coefficient, since it works with the 6th power of the distance from the distortion centre compared to the 4th power which K_2 scales. This allows the true minimum to be found more easily.

In this paper a numerical method was deemed to have converged if the norm of the gradient was less than $\sqrt{n}10^{-6}$ (where n is the number of parameters in the function being minimized) or the step size was less than 10^{-8}. The former criterion is a function of n so that as the number of parameters increases, the required average magnitude of each element in the gradient vector remains constant. A centered gradient calculation was employed; this requires $2n$ function calls instead of the $n+1$ function calls of the more common forward gradient method. However, it provides an approximation of $\bigtriangledown f$ at the point concerned instead of a collection of partial derivatives each offset by half the gradient step in their respective dimensions.

4. RESULTS AND ANALYSIS

Table 1 and Table 2 provide the results for the characterizations of the two different lenses considered in this work. The distortion results listed are the average distortion metrics, as per Eq. 6, expressed in pixels and the skewness calculated as per Eq. 7 expressed in degrees. The uncompensated distortion for lenses of Type A is 1.768 pixels RMS. Type A lenses were designed to have optically less distortion than Type B lenses whose average uncompensated distortion is 4.302 pixels RMS. Table 3 express the improvement in the distortion characterization achieved by the angular gain models compared to a nuity angular gain.

The tables show that both angular gain functions improve the distortion characterization. This is particularly true for the simple first order models where improvements of up to 75% were obtained using sinusoidal gain, although this was at the expense of a higher induced trapezoidal skewness compared to the elliptical gain. For the five models which contained at least a second order radial component, the improvement varied from 3% to 15% with both variable angular gain models exhibiting acceptable skewnesses. The differing results for the low order models between the two lens types show that no single lens distortion model can be universally applied, but rather, critical thinking and analysis are required so that the desired level of distortion characterization is achieved. Regarding distortion models with one radial term and no tangential terms, Tsai[2] famously stated that "any more elaborate modeling not only would not help but would cause numerical instability." Compared to this, an improvement of over 79% has been demonstrated.

Table 1. Results for Lens Type A

Distortion Model				Angular Gain				
Model Number	Radial Terms	Tangential Terms	Optimal Center Found	Constant	Elliptical		Sinusoidal	
				Dist.	Dist.	Skewness	Dist.	Skewness
1	1	0	N	0.2130	0.1059	0.294°	0.0801	5.840°
2	1	0	Y	0.1312	0.1033	0.310°	0.0787	5.874°
3	2	0	Y	0.0597	0.0578	0.206°	0.0565	0.356°
4	3	2	N	0.0703	0.0580	0.203°	0.0592	0.351°
5	3	2	Y	0.0595	0.0572	0.210°	0.0544	0.360°
6	3	3	Y	0.0595	0.0569	0.273°	0.0541	0.360°
7	5	0	N	0.0703	0.0580	0.210°	0.0592	0.351°

Table 2. Results for Lens Type B

Distortion Model				Angular Gain				
Model Number	Radial Terms	Tangential Terms	Optimal Center Found	Constant	Elliptical		Sinusoidal	
				Dist.	Dist.	Skewness	Dist.	Skewness
1	1	0	N	0.3038	0.3014	0.203°	0.0774	9.500°
2	1	0	Y	0.2487	0.1860	0.207°	0.0723	9.499°
3	2	0	Y	0.0750	0.0664	0.223°	0.0727	0.996°
4	3	2	N	0.0715	0.0655	0.230°	0.0628	0.889°
5	3	2	Y	0.0673	0.0646	0.214°	0.0625	0.829°
6	3	3	Y	0.0670	0.0639	0.230°	0.0622	0.871°
7	5	0	N	0.0714	0.0654	0.220°	0.0623	0.885°

Table 3. Percentage improvements using variable angular gains

Distortion Model				Angular Gain			
Model Number	Radial Terms	Tangential Terms	Optimal Center Found	Elliptical		Sinusoidal	
				Type A	Type B	Type A	Type B
1	1	0	N	50.2%	0.9%	62.2%	75.7%
2	1	0	Y	21.4%	25.3%	39.3%	71.0%
3	2	0	Y	3.2%	11.2%	5.4%	3.1%
4	3	2	N	15.4%	8.3%	14.4%	12.0%
5	3	2	Y	3.9%	3.9%	8.8%	7.0%
6	3	3	Y	4.4%	4.6%	9.4%	7.2%
7	5	0	N	15.4%	8.3%	14.5%	12.6%

5. CONCLUSION

This paper addresses the issue of the implicit radial symmetry for the radial components of the predominant Conrady/Brown model. It showed that extending the model with an angular gain decreased the residual distortion of low-order models by up to 75%. The most complicated models, which only recently were reliably and successfully applied, also benefits by a 4% to 10% improvement.

Elliptical distortion, which models the non-orthogonality of the image plane, was seen to always enhance the distortion characterization without inducing unwanted trapezoidal distortion. Sinusoidal distortion was seen to provide improved distortion characterization beyond even what the elliptical radial achieved, at least in terms of output line straightness. However this technique may require some care when applied to low order models.

A new tool has been created which can provide extremely accurate distortion characterization. This allows high-end photogrammetric applications to improve their accuracy even if they already use complex models. Similarly, low-end cameras and lenses (such as those found on mobile phones) whose production may not be as carefully controlled, can benefit by using the elliptical variable angular gain and make use of the ever increasing processing power commonly available on such devices.

REFERENCES

[1] de Villiers, J., "Real-time stitching of high resolution video on COTS hardware," in [*Proceedings of the 2009 International Symposium on Optomechatronic Technologies*], *ISOT2009* **9**, 46–51 (2009).

[2] Tsai, R., "A versatile camera calibration technique for high-accuracy 3D machine vision metrology using off-the-shelf tv cameras and lenses," *IEEE Journal of Robotics and Automation* **3**, 323–344 (1987).

[3] de Villiers, J., [*Correction of radially asymmetric lens distortion with a closed form solution and inverse function, Master's thesis*], University of Pretoria, Pretoria, RSA (2008).

[4] Conrady, A., "Decentered lens systems," *Monthly Notices of the Royal Astronomical Society* **79**, 384–390 (1919).

[5] Brown, D., "Decentering distortion of lenses," *Photogrammetric Engineering* **7**, 444–462 (1966).

[6] Brown, D., "Close range camera calibration," *Photogrammetric Engineering* **8**, 855–855 (1971).

[7] de Villiers, J., Leuschner, F., and Geldenhuys, R., "Centi-pixel accurate real-time inverse distortion correction," in [*Proceedings of the 2008 International Symposium on Optomechatronic Technologies*], *ISOT2008* **7266**, 1–8 (2008).

[8] Snyman, J., "An improved version of the original leap-frog dynamic method for unconstrained minimization: LFOP1(b)," *Applied Mathematics and Modelling* **7**, 216–218 (1983).

[9] Snyman, J., [*Practical Mathematical Optimization*], Springer, New York, USA (2005).